Proceedings of the 12th International Conference on Fluid Flow, Heat and Mass Transfer (FFHMT 2025)
July 15, 2025 - July 17, 2025 | Imperial College London Conference, London, United Kingdom
Paper No. 159
DOI: 10.11159/ffhmt25.159

Thermal Performance Optimization of Lithium-Ion Battery Pack: A Numerical Study

Roshan Devidas Bhagat[1], Samir Deshmukh[2],
[1]Symbiosis Skills and Professional University
Kiwale, Pune, India
roshan.bhagat@sspu.ac.in ; sjdeshmukh@mitra.ac.in
[2]Prof Ram Meghe Institute of Technology & Research
Badnera, Amravati, India

Abstract – Thermal Management of Lithium-Ion battery pack is increasingly gaining importance in line with recent advancement in electric vehicle technology. Lithium-ion batteries are most widely used in electric vehicle as source of power. Lithium-ion cells are connected in series and parallel to achieved the power requirement of an electric vehicle. Lithium-ion cells generates heat during their high-end operations, this generated heat causes thermal runway, capacity loss and hence need to be dissipated to the surrounding so as to ensure the longer life span and to optimize the performance of battery pack. A three dimensional (3D) Numerical model of lithium-ion battery pack is investigated to understand the temperature distribution along the battery pack with water and air used as working fluid. The purpose of numerical analysis is to investigate the temperature distribution and optimize the performance of battery pack through carefully controlled parameter which subsequently reduce the cost of experimentation. This numerical result can further be used as reference while designing the battery pack for electric vehicle.

***Keywords*:** Thermal management, lithium ion, battery pack, electric vehicle

1. Introduction

Thermal management of electric vehicle is currently the topic of concern with recent advancement in electric vehicle (EV) technology. Worldwide transportation vehicles are still heavily dependent on fuels like petrol and diesel for day-to-day operation, which increases the levels of harmful emissions. Three to five percent of the vehicles use alternative fuels like ethanol and natural gas, while about 90% of them run on petroleum products [1]. Battery-operated cars known as Electric cars (EVs), another alternative to conventional fuels, have garnered growing attention in the recent years [2-3]. Electric Vehicles (EVs) have a lower centre of gravity than traditional combustion engine-based vehicles, making them safer [4]. Electric Vehicles (EVs) are also appealing since they may deliver instant torque and have lower operating and maintenance expenses than cars with internal combustion engines [4-5] Stacks of rechargeable lithium-ion batteries (LIBs), which are commonly used in EVs, provide the energy needed to power an induction motor that propels the vehicles while they are in motion [6-7]. The price and lifespan of the battery pack that powers an electric vehicle (EV) are the main factors affecting its cost and lifespan [12-14]. About 35% of the total cost structure of an EV is made up of batteries [15-16]. The surrounding temperature of a battery is the most significant factor that affects battery's life [8]. The optimal temperature range for lithium-ion batteries is 25^0C to 40^0C, while the acceptable temperature range has been reported to be between -30^0C and 60^0C [12,15] However, during normal EV operation, temperatures can rise above 60^0C for extended periods of time, which can be disastrous for the health of the battery [10].

2. Geometry and Physical Attributes

2.1. Geometry

The geometry of 18 cell lithium-ion battery pack with water and air as working fluid is prepared with Ansys design modeler. The geometry is slice to define the presence of lithium battery and the working fluid used are water liquid and air.

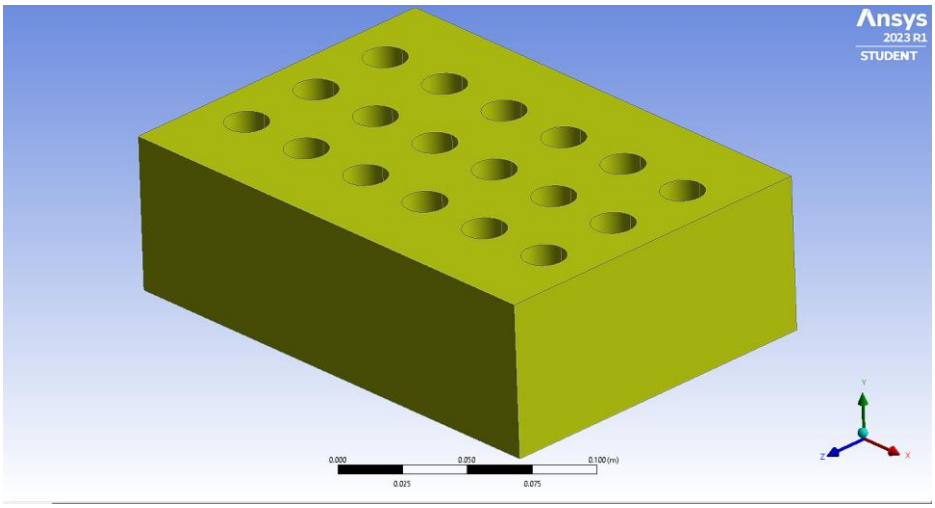

Fig 1: Numerical model of lithium-ion battery pack with air as working fluid

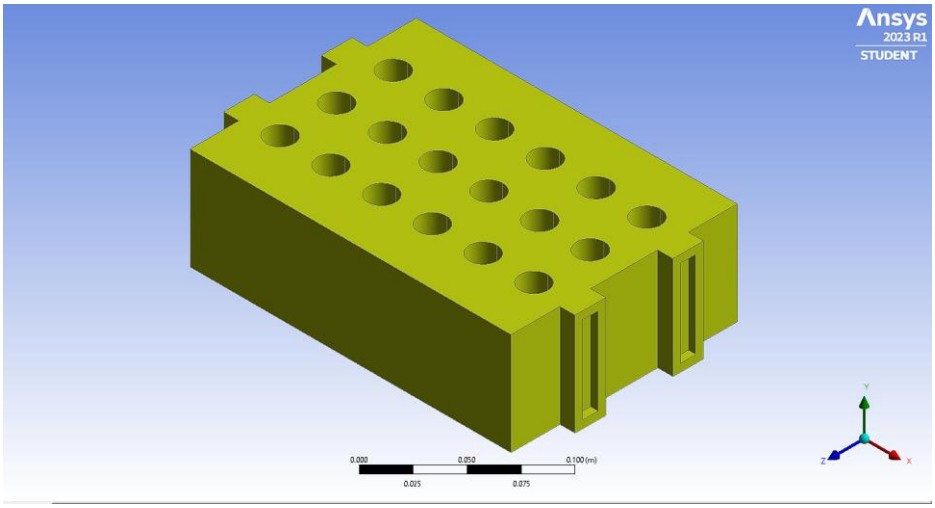

Fig 2: Numerical model of lithium-ion battery pack with water as working fluid

The figure 1 and figure 2 shows the numerical model generated with the help of Ansys design modeler. Figure 1 represent numerical model for air as working fluid whereas, figure 2 represent numerical model for water as working fluid. The 3D computational domain has 18 cells, the boundary conditions will be applied on the wall of the cell.

2.2. Physical Characteristics of Lithium-Ion Battery Pack

Table 1 Specification of the battery pack

Sr. No.	Parameter	Value
1	Number of Cells	18 Units
2	Nominal Battery pack voltage	24 Volts
3	Nominal battery capacity	187.2 Whr

Table 2 Specification of the Lithium Cell

Sr. No.	Parameter	Value
1	Nominal voltage	3.7 Volts
2	Cell Weight	48 g
3	Nominal Capacity	2600 mAh
4	Maximum charging current	1C
5	Maximum discharging current	3C
6	Anode material	Graphite

3. Mesh Generation and Quality Check

The Mesh is generated with meshing tool available in Ansys workbench. Figure 3 and 4 shows the mesh generated on 3D computational domain with help of meshing tool in Ansys workbench

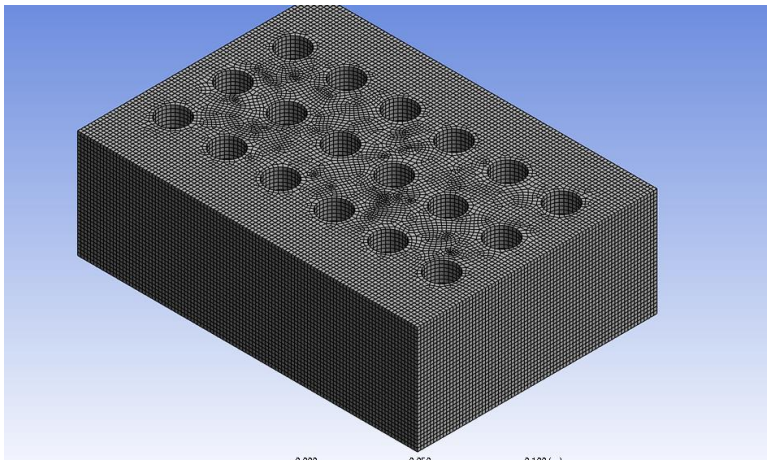

Fig 3: Mesh generated on numerical model of lithium-ion battery pack with air as working fluid.

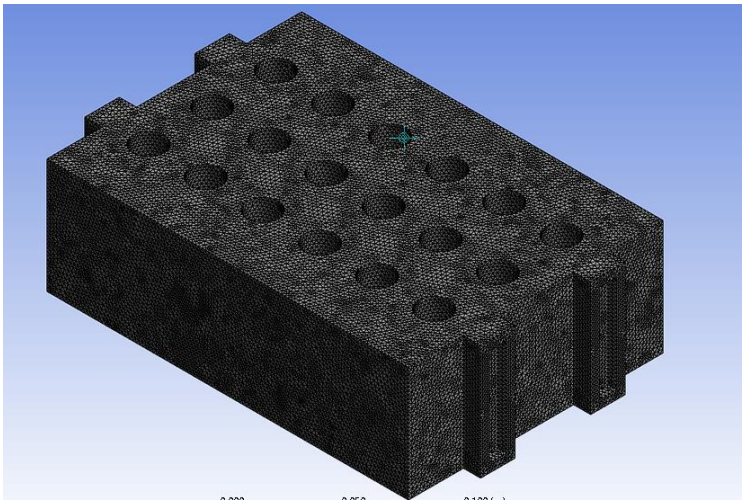

Fig 4: Mesh generated on numerical model of lithium-ion battery pack with water as working fluid.

3.1. Details of Mesh with Water as Working Fluid.

Table 3: Details of mesh on battery pack with water as working fluid

Sr. No.	Domain	Nodes	Element
1	Battery Pack	189517	983833

3.2. Details of Mesh with Air as Working Fluid.

Table 4: Details of mesh on battery pack with air as working fluid

Sr. No.	Domain	Nodes	Element
1	Battery Pack	256700	236313

3.3. Mesh Quality Check

Structured grid is generated and element size of 0.003 is taken for study. The element size is selected taking into consideration the student version of Ansys used for generating simulation result.

3.4. Mesh Independent Study

To check the accuracy of CFD simulation it is necessary to perform the mesh independence study. The mesh is generated for three difference sizes i.e., course, medium and fine. The time required for CFD simulation depends on the mesh size selected. While proceeding for simulation it was ensured to have skewness near to '0' and orthogonal quality near to '1'. The mesh generated satisfying the above criterion is selected for simulation. The selection of mesh also ensured to keep the Courant Number to a lower value to avoid the divergence in the velocity field. CFD simulation is performed with student version of Ansys keeping in mind limitation nodes and element and computational time required.

4. Boundary Conditions

The boundary conditions involve the velocity of fluid entering the computational domain and the temperature of cell wall. The cell wall acts as heat source, whereas fluid absorbs the heat rejected from cell wall.

Table 5: Boundary conditions on computational domain

Sr. No.	Boundary Condition	Value
1	Velocity at Inlet	1 m/s
2	Temperature of cell wall	303 K

4.1. Model and Material Selection

Energy equation is turned on, standard k-∈ model with enhanced wall treatment and thermal effect are taken into consideration. Air and water are respectively defined as working fluid.

4.2. Phase Definition on 3D Computational Domain

The 3D computational domain is defined with fluid zones to apply boundary condition. The fluid zones are respectively defined by working fluid as air and water for separate case of simulation.

4.3. Setting Cell Zone Conditions on Computational Domain

The operating pressure of 101325 Pa is set on the 3D computational domain. Pressure based solver with gravity of 9.8 m/s^2 is taken into consideration as the flow of fluid takes place from inlet to outlet.

4.4. Setting Initialization and Patch

Standard initialization is taken into consideration with computation starting from inlet, reference frame is considered relative to cell zone.

4.5. Simulation Setup

Solution animation for contours of static temperature, contours of wall temperature are set, fixed time steps are selected with time step size of 0.1. The maximum iteration for time step is 20.

5. CFD Simulation

The CFD simulation is performed with water and air as working fluid in order the understand the heat transfer from cell wall to the working fluid.

5.1. CFD Simulation with Air as Working Fluid

5.1.1 Contours of Static Temperature

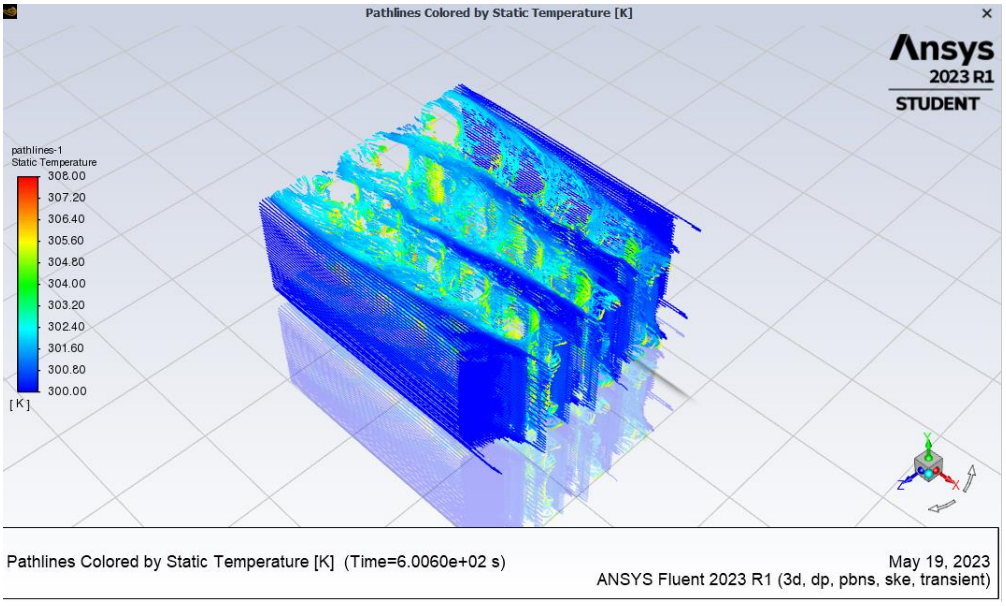

Fig 5: Contours of static temperature along the length of battery pack with air as working fluid

The 3D visualization shows path lines coloured by static temperature for a battery pack that is being cooled using air as the working fluid. The color scale on the left indicates temperature values ranging from 300 K (cool, blue) to 308 K (hot, red). The simulation has been run for a time value of 606 seconds, representing a quasi-steady-state condition. The blue and green regions dominate most of the visualization, indicating that a significant portion of the battery pack is being maintained at a cooler temperature closer to 300 K to 304 K. Warmer zones (yellow to red) can be observed along specific regions within the battery pack, suggesting areas where heat accumulation is higher. The presence of hotter zones indicates that these areas receiving less airflow or experiencing higher heat generation from the battery cells. The path lines show how air is flowing through the channels between the battery cells. The visualization highlights how air interacts with the battery surfaces, absorbing heat and carrying it away. The cooler air entering the system reduces the temperature of the battery cells, but there are still some localized hot spots, particularly around the centre and near the cells where airflow may be restricted. The flow patterns suggest that air is effectively cooling the outer regions of the pack, but the central regions may not be receiving sufficient cooling.

5.1.2. Contours of Wall Temperature

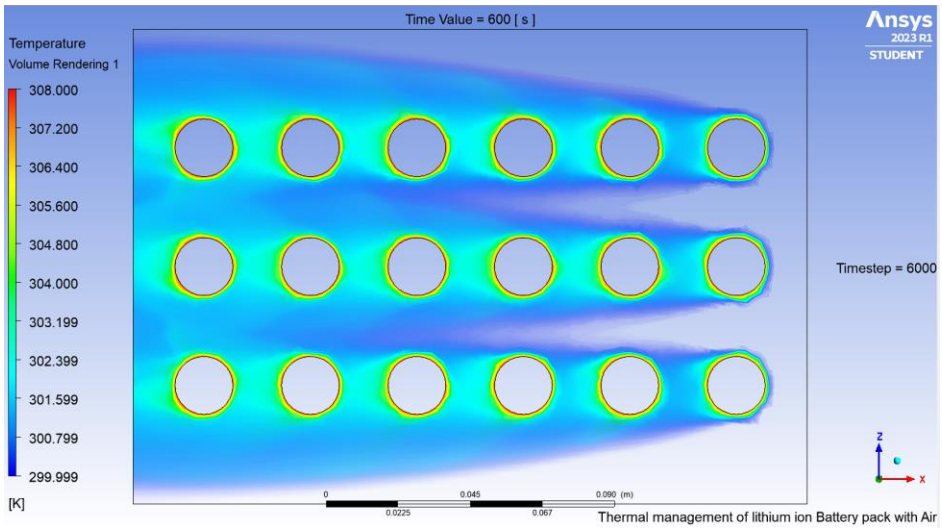

Fig 6: Contours of wall temperature along the length of battery pack with air as working fluid

This 2D visualization shows the temperature distribution on a lithium-ion battery pack using air cooling at steady-state after 600 seconds. The color scale ranges from 299.999 K (blue) to 308.000 K (red). Cooler regions (blue-green, 300–305 K) dominate around the cylindrical cells, while warmer zones (yellow-red) indicate heat accumulation, especially near the outer edges. Red rings highlight hot spots reaching 308 K. The air-cooling system effectively lowers temperatures near the edges but struggles in central areas due to restricted airflow, leading to localized heat build-up. Air cooling, though cost-effective, has limitations for densely packed batteries. Enhancing airflow distribution could improve temperature uniformity and reduce thermal stress. The system keeps temperatures below 308 K, ensuring battery safety and efficiency.

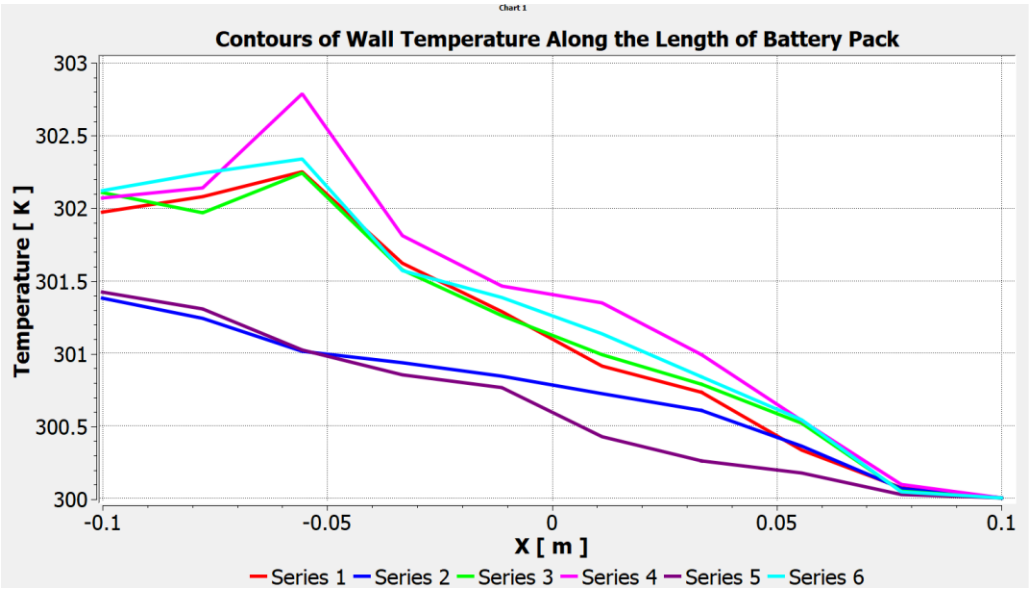

Fig 7: Variation of wall temperature along the length of battery pack.

The graph illustrates the temperature distribution along the battery pack's length (-0.1 m to 0.1 m). The y-axis shows temperature (300 K to 303 K), with multiple series representing different locations or conditions. A temperature drop at the edges suggests effective heat dissipation, likely due to airflow or heat sinks. The central peak indicates less effective cooling, highlighting the need for design optimization.

5.2. CFD Simulation with Water as Working Fluid

5.2.1 Contours of Static Temperature

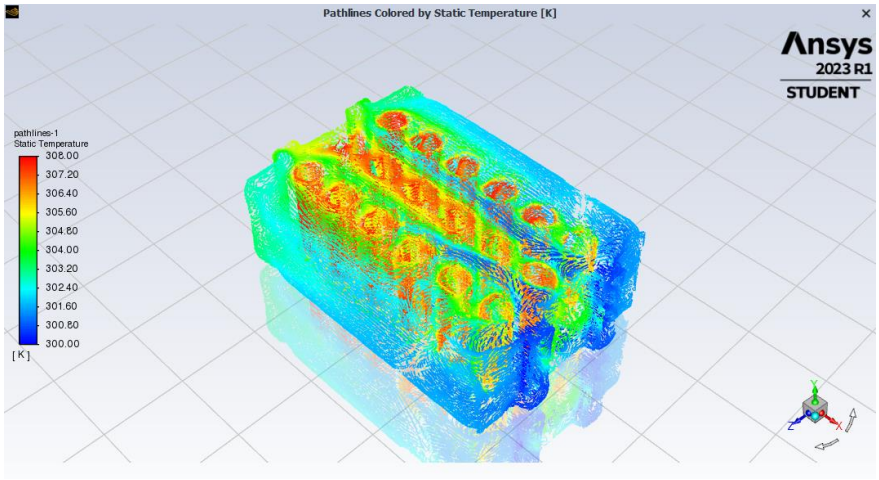

Fig 8: Contours of static temperature along the length of battery pack with water as working fluid

The 3D visualization shows path lines coloured by static temperature for a water-cooled lithium-ion battery pack, simulated in Ansys fluent at steady-state after 606 seconds. The colour scale (300 K to 308 K) indicates effective cooling, with blue and green dominating most regions. Localized hot spots (yellow-red) suggest minor heat accumulation, mainly in central cells due to restricted water flow. Water cooling, with its superior thermal properties, ensures better thermal management than air cooling. Smooth temperature gradients confirm efficient heat absorption and dissipation by the water flow.

5.2.2. Contours of Wall Temperature

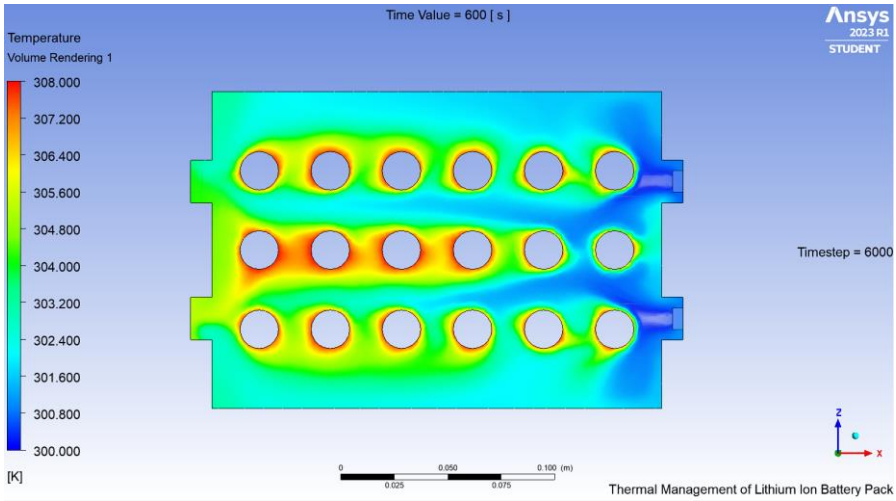

Fig 9: Contours of wall temperature along the length of battery pack with water as working fluid.

This 2D visualization shows temperature contours for a water-cooled lithium-ion battery pack at steady-state after 600 seconds. The temperature scale ranges from 300 K (blue, cooler) to 308 K (red, hotter). Water cooling ensures effective heat removal, maintaining a uniform temperature with fewer hot spots. Localized heat accumulation (yellow-red) appears around central cells due to restricted flow. Water efficiently cools the cells from both sides, with edges and inlet/outlet regions remaining cooler (blue), indicating effective heat dissipation.

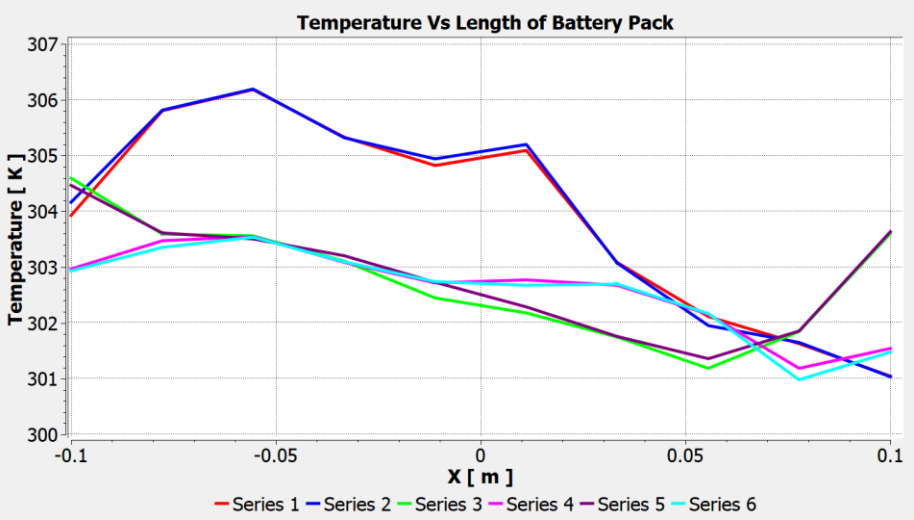

Fig 10: Contours of Wall temperature along the length of battery pack with water as working fluid.

The graph shows the temperature profile along a water-cooled lithium-ion battery pack (-0.1 m to 0.1 m). The y-axis ranges from 301 K to 307 K, with multiple series representing different positions. Temperature peaks (around -0.05 m to 0 m) reach nearly 306 K in Series 1 (red) and Series 2 (blue), indicating heat accumulation. Towards the ends, temperatures drop below 302 K. Series 4 (green) and Series 6 (purple) show better cooling performance, maintaining lower temperatures and highlighting effective heat dissipation in those areas.

6. Experimentation

6.1. Details of Experimental Setup

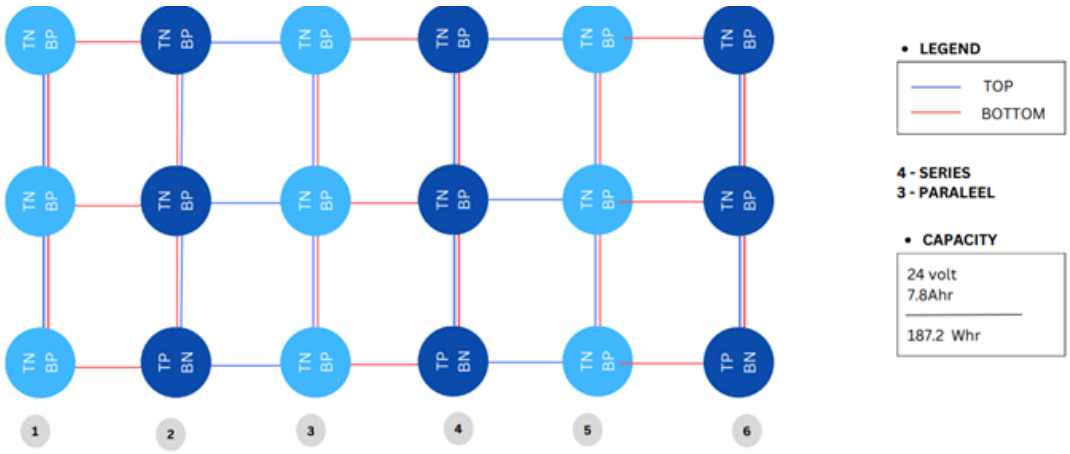

Fig 11: Wiring diagram for lithium-ion battery pack

6.2. Experimentation with Air and Water as Working Fluid

Table 6: Lithium-ion cell temperature with air and water flow at 01 m/s

Sr. No.	Time in Seconds	With no air flow		With air flow at 01 m/s		With water flow at 01 m/s	
		Cell Temperature (LHS) in^0C	Cell Temperature (RHS) in^0C	Cell Temperature (LHS) in^0C	Cell Temperature (RHS) in^0C	Cell Temperature (LHS) in^{0}C	Cell Temperature (RHS) in^{0}C
1	0 Seconds	$S_1 = 31^0C$	$S_1 = 31^0C$	$S_1 = 31^0C$	$S_1 = 31^0C$	$S_1 = 31.6^0C$	$S_1 = 31.5^0C$
		$S_3 = 31^0C$	$S_3 = 31^0C$	$S_3 = 31^0C$	$S_3 = 31^0C$	$S_3 = 31.4^0C$	$S_3 = 31.4^0C$
		$S_5 = 31^0C$	$S_5 = 31^0C$	$S_5 = 31^0C$	$S_5 = 31^0C$	$S_5 = 31.5^0C$	$S_5 = 31.4^0C$
2	120 Seconds	$S_1 = 31.8^0C$	$S_1 = 32.1^0C$	$S_1 = 31.5^0C$	$S_1 = 31.5^0C$	$S_1 = 31.5^0C$	$S_1 = 31.6^0C$
		$S_3 = 31.8^0C$	$S_3 = 32.1^0C$	$S_3 = 31.5^0C$	$S_3 = 31.5^0C$	$S_3 = 31.6^0C$	$S_3 = 31.5^0C$
		$S_5 = 31.8^0C$	$S_5 = 32^0C$	$S_5 = 31.5^0C$	$S_5 = 31.5^0C$	$S_5 = 31.6^0C$	$S_5 = 31.5^0C$
3	240 Seconds	$S_1 = 31.9^0C$	$S_1 = 32.2^0C$	$S_1 = 31.4^0C$	$S_1 = 31.3^0C$	$S_1 = 31.5^0C$	$S_1 = 31.5^0C$
		$S_3 = 32.5^0C$	$S_3 = 32.1^0C$	$S_3 = 31.4^0C$	$S_3 = 31.3^0C$	$S_3 = 31.5^0C$	$S_3 = 31.5^0C$
		$S_5 = 33.3^0C$	$S_5 = 32.8^0C$	$S_5 = 31.6^0C$	$S_5 = 31.3^0C$	$S_5 = 31.5^0C$	$S_5 = 31.5^0C$
4	360 Seconds	$S_1 = 32.4^0C$	$S_1 = 32^0C$	$S_1 = 31.4^0C$	$S_1 = 31.2^0C$	$S_1 = 31.2^0C$	$S_1 = 31.4^0C$
		$S_3 = 32^0C$	$S_3 = 32.1^0C$	$S_3 = 31.4^0C$	$S_3 = 31.3^0C$	$S_3 = 31.3^0C$	$S_3 = 31.3^0C$
		$S_5 = 32^0C$	$S_5 = 32^0C$	$S_5 = 31.4^0C$	$S_5 = 31.4^0C$	$S_5 = 31.4^0C$	$S_5 = 31.4^0C$
5	480 Seconds	$S_1 = 32.2^0C$	$S_1 = 32.1^0C$	$S_1 = 31.5^0C$	$S_1 = 31.3^0C$	$S_1 = 31.2^0C$	$S_1 = 31.3^0C$
		$S_3 = 32.2^0C$	$S_3 = 32.1^0C$	$S_3 = 31.3^0C$	$S_3 = 31.4^0C$	$S_3 = 31.2^0C$	$S_3 = 31.3^0C$
		$S_5 = 32.1^0C$	$S_5 = 32.2^0C$	$S_5 = 31.3^0C$	$S_5 = 31.4^0C$	$S_5 = 31.2^0C$	$S_5 = 31.2^0C$
6	600 Seconds	$S_1 = 32^0C$	$S_1 = 32^0C$	$S_1 = 31.7^0C$	$S_1 = 31.3^0C$	$S_1 = 31.1^0C$	$S_1 = 31.3^0C$
		$S_3 = 32^0C$	$S_3 = 32^0C$	$S_3 = 31.4^0C$	$S_3 = 31.3^0C$	$S_3 = 31.3^0C$	$S_3 = 31.3^0C$
		$S_5 = 31.8^0C$	$S_5 = 32^0C$	$S_5 = 31.3^0C$	$S_5 = 31.3^0C$	$S_5 = 31.3^0C$	$S_5 = 31.4^0C$

The table systematically presents temperature variations over time (0 to 600 seconds) for different cooling methods, with measurements taken at multiple cell positions on both the left-hand side (LHS) and right-hand side (RHS). It highlights that, in all cases, temperatures increase with time, but the rate of increase is significantly lower with air and water cooling. Notably, water cooling maintains nearly uniform temperatures across all positions, while air cooling shows slight variations, and no airflow results in the highest temperature differences.

The experimental results compare lithium-ion cell temperatures under three cooling conditions: no airflow, air cooling at 01 m/s, and water cooling at 01 m/s. Without airflow, temperatures gradually increase over time, reaching up to 33.3℃, indicating inefficient heat dissipation. With air cooling, the maximum temperature is reduced to 32℃, showing moderate improvement in heat removal, but some heat accumulation still occurs. Water cooling proves to be the most effective, maintaining a peak temperature of 31.5℃, demonstrating superior thermal management. The data reveals that without any cooling, the battery cells experience significant temperature rise, which can impact performance and longevity. Air cooling helps mitigate the temperature increase but is less efficient due to air's lower thermal conductivity. Water cooling provides the most uniform temperature distribution, preventing excessive heat build-up, particularly in central regions where heat accumulation is common. The temperature variations are minimal in water cooling, ensuring better thermal stability. The results emphasize that while air cooling is a feasible and cost-effective solution, water cooling is more reliable for managing battery pack temperatures. Effective cooling strategies are crucial for enhancing battery safety, performance, and lifespan, especially in high-power applications.

7. Result and Discussion

7.1 Experimental Vs CFD Results

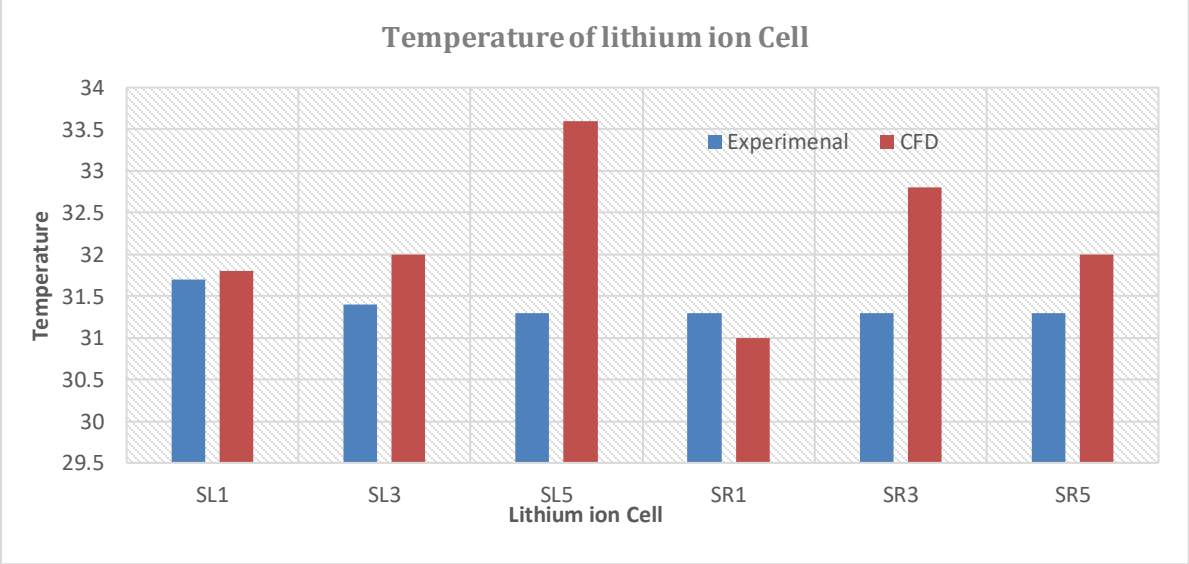

Fig 12: Experimental v/s CFD result with air as working fluid.

The graph compares the temperatures of various lithium-ion cells (SL1, SL3, SL5, SR1, and SR5) obtained from both experimental measurements and CFD simulations when air is used as the cooling fluid. Experimental temperatures (orange bars) are generally higher than the CFD-simulated temperatures (blue bars). The most significant temperature difference is observed in cell SL5, where the experimental result shows a higher temperature compared to the CFD simulation. The temperature distribution across all cells shows that both experimental and CFD results follow a similar trend, though experimental values are slightly elevated.

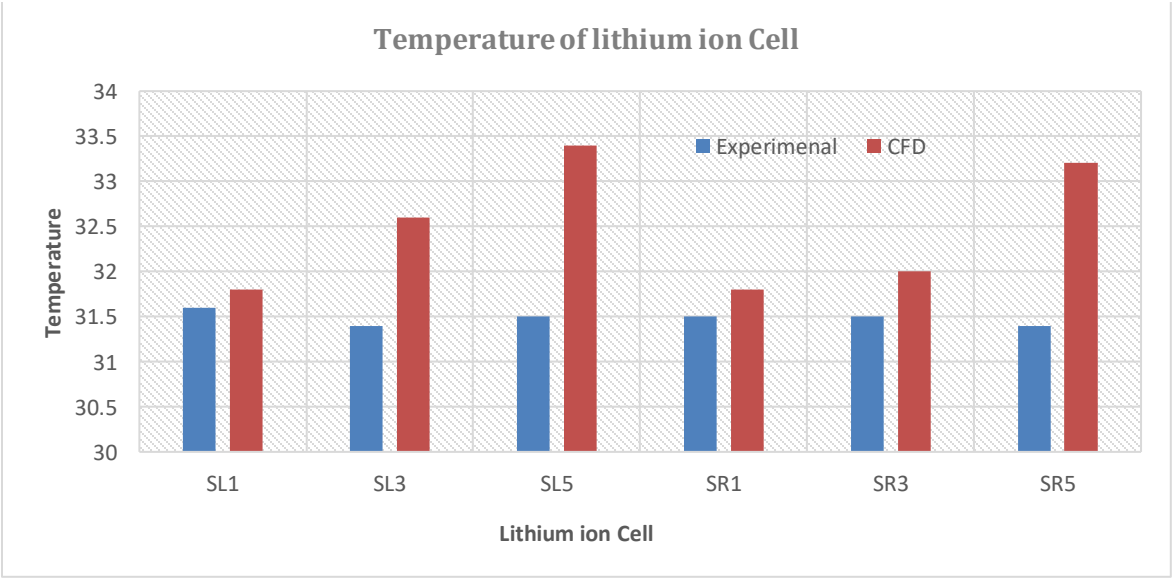

Fig 13: Experimental v/s CFD result with water as working fluid.

This figure compares the experimental and CFD results for the same set of lithium-ion cells, but with water used as the cooling fluid. The experimental and CFD temperatures are much closer when using water compared to air, indicating better agreement between simulation and experimental results. The temperature discrepancies between experimental and CFD results are less pronounced, especially for cells SL1, SL3, and SR1. Cell SL5 still shows the highest temperature in both experimental and CFD results, but the difference between the two is smaller than when air was used.

7.2 Discussion

From figure 12 experimental and CFD result for air as working fluid comply each other at few points on lithium-ion cell namely SL1, SL3, SR1 and SR5. Whereas, considerable variations are observed at SL5 and SR3. From figure 13 experimental and CFD result with water as working fluid comply each other at few points on lithium-ion cell namely SL1, SR1 and SR3. Whereas, deviations are observed at SL3, SL5 and SR5.

8. Conclusion and Future Scope

8.1 Conclusion

After performing the experimentation on water and air as working fluid with subsequent CFD analysis following points are concluded. Water as a cooling fluid is significantly more effective than air, as evidenced by the lower temperature differences between experimental and CFD results. Water's higher thermal conductivity and heat capacity lead to better heat dissipation, resulting in more uniform and lower temperatures across the cells. The CFD simulations provide a good approximation of the experimental results, especially when water is used as the cooling fluid. The larger deviations seen with air as the cooling fluid may be due to factors not fully captured in the CFD model, such as turbulence or non-uniform airflow. For battery packs that generate significant heat, using water as the cooling fluid is recommended to ensure better thermal management and prevent overheating. Improving the CFD model to account for airflow complexities could enhance the accuracy of simulations for air-cooled systems.

8.2 Scope for Future Work

After analysing the experimental and CFD result, the research work can be extended by implementing the following. The numerical model can be tested with finer mesh size to have more accurate result in order to predict the thermal performance of lithium-ion battery pack. Use of different working fluid with higher heat carrying capacity to extract heat from lithium-ion cell. By varying the spacing between two subsequent lithium-ion cells to have higher heat transfer rate from cell wall to the fluid. By introducing working fluid in the later part of lithium-ion battery pack to have effective heat transfer from cell wall to working fluid.

References

[1] J. Sanguesa, V. Torres-Sanz, P. Garrido, F. Martinez, J. Marquez-Barja, "A review on electric vehicles: technologies and challenges," Smart Cities 4 (1) (2021) 372–404, https://doi.org/10.3390/smartcities4010022

[2] D. Pelegov, J. Pontes, Main drivers of battery industry changes: electric vehicles—a market overview, Batteries 4 (4) (2018) 65., https://doi.org/10.3390/batteries4040065

[3] H. Mazumder, M.M.A.E. Hassan, M. Ektesabi, A. Kapoor, "Performance analysis of EV for different mass distributions to ensure safe handling," Energy Procedia 14 (2012) 949–954, https://doi.org/10.1016/j.egypro.2011.12.1038

[4] F. Un-Noor, S. Padmanaban, L. Mihet-Popa, M. Mollah, E. Hossain, "A comprehensive study of key electric vehicle (EV) components, technologies, challenges, impacts, and future direction of development," Energies 10 (8) (2017) 1217, https://doi.org/10.3390/en10081217

[5] S. Sharma, A.K. Panwar, M.M. Tripathi, "Storage technologies for electric vehicles," J. Traffic Transport. Eng. (English Ed.) 7 (3) (2020) 340–361, https://doi.org/10.1016/j.jtte.2020.04.004

[6] A.A. Pesaran, "Battery thermal models for hybrid vehicle simulations," J. Power Sources 110 (2) (2002) 377–382, http://dx.doi.org/10.1016/S0378-7753(02)00200-8

[7] Hofmann, N. Uhlmann, C. Ziebert, O. Wiegand, A. Schmidt, T. Hanemann, "Preventing Li-ion cell explosion during thermal runaway with reduced pressure, Appl. Therm. Eng. 124 (2017) 539–544, http://dx.doi.org/10.1016/j.applthermaleng.2017.06.056
[8] J. Jacob, "The chalkboard: C rating of batteries: a misleading concept, C flux rather than C rate," Electrochem. Soc. Interface 27 (2) (2018) 42–43, http://dx.doi.org/10.1149/2.F01182if
[9] Z. Rao, S. Wang, "A review of power battery thermal energy management," Renew. Sustain. Energy Rev. 15 (9) (2011) 4554–4571, http://dx.doi.org/10.1016/j.rser.2011.07.096
[10] K. Jiang, G. Liao, F. Zhang, J. Chen, E. Leng, "Thermal management technology of power lithium-ion batteries based on the phase transition of materials: a review," J. Storage Mater. 32 (2020), 101816, https://doi.org/10.1016/j.est.2020.101816
[11] M. Zhi, R. Fan, X. Yang, L. Zheng, S. Yue, Q. Liu, "Recent research progress on phase change materials for thermal management of lithium-ion batteries," J. Energy Storage. 45 (2022) 103694, https://doi.org/10.1016/j.est.2021.103694.
[12] B. Wang, C. Ji, S. Wang, J. Sun, S. Pan, D. Wang, C. Liang, "Study of non-uniform temperature and discharging distribution for lithium-ion battery modules in series and parallel connection," Appl. Therm. Eng. 168 (2020) 114831, https://doi.org/10.1016/j.applther- maleng.2019.114831.
[13] Y. Zhang, J. Huang, M. Cao, Z. Liu, Q. Chen, "A novel flexible phase change material with well thermal and mechanical properties for lithium batteries application," J. Energy Storage. 44 (2021) 103433, https://doi.org/10.1016/j.est.2021.103433
[14] N. Yang, X. Zhang, G. Li, D. Hua, "Assessment of the forced air-cooling performance for cylindrical lithium-ion battery packs: a comparative analysis between aligned and staggered cell arrangements," Appl. Therm. Eng. 80 (2015) 55–65, https://doi.org/10.1016/j. applthermaleng.2015.01.049
[15] J. Zhao, Z. Rao, Y. Li, "Thermal performance of mini-channel liquid cooled cylinder-based battery thermal management for cylindrical lithium-ion power battery," Energy Conversion Management 103 (2015) 157–165, https://doi.org/10.1016/j.enconman.2015.06.056
[16] L.H. Saw, Y. Ye, A.A.O. Tay, W.T. Chong, S.H. Kuan, M.C. Yew, "Computational fluid dynamic and thermal analysis of Lithium-ion battery pack with air cooling," Applied Energy 177 (2016) 783–792, https://doi.org/10.1016/j.apenergy.2016.05.122.
[17] J. Jaguemont, L. Boulon, Y. Dube, "A comprehensive review of lithium-ion batteries used in hybrid and electric vehicles at cold temperatures," Appl. Energy 164 (2016) 99–114, https://doi.org/10.1016/j.apenergy.2015.11.034.
[18] L.H. Saw, Y.J. King, M.C. Yew, T. Ching Ng, W.T. Chong, N.A. Pambudi, "Feasibility study of mist cooling for lithium-ion battery," Energy Procedia 142 (2017) 2592–2597, https://doi.org/10.1016/j.egypro.2017.12.197.